

Authors: R.J. Nijboer, G. van Diepen	Date of issue: 2012-06-26 Kind of issue: public	Scope: Doc.id:	ASTRON
	Status: final Revision nr: 1.0		




Imaging while correcting for Direction Dependent Effects

ALBiUS Deliverable for subtask 6.2.5



© ASTRON 2012

All rights are reserved. Reproduction in whole or in part is prohibited without written consent of the copyright owner.

Authors: R.J. Nijboer, G. van Diepen	Date of issue: 2012-06-26 Kind of issue: public	Scope: Doc.id:	
	Status: final Revision nr: 1.0		




Authors: R.J. Nijboer, G. van Diepen	Date of issue: 2012-06-26 Kind of issue: public	Scope: Doc.id:	
	Status: final Revision nr: 1.0		

Table of contents:

1	Introduction	5
1.1	Acknowledgements	5
2	Direction Dependent Effects	6
2.1	Non-coplanar baselines	6
2.2	Primary Beams	6
2.3	Ionosphere	7
2.4	Correction methods	8
3	Implementation of AW-Projection	10
3.1	Extending the CASA implementation	10
3.2	Parallelised and distributed processing	11
3.3	Optimization: FFT or direct convolution	11
3.4	LOFAR Optimization: splitting array factor and element beam	12
3.5	LOFAR Optimization: ignoring very high w-values	13
3.6	Test results	13
4	Code manual	18
4.1	Background	18
4.2	Usage	18
4.3	Output files	18
4.4	Parameters	18
5	Future work	20
5.1	Further computational optimizations	20
5.2	Correction for ionospheric effects	21
6	Conclusions	22
7	References	23

Authors: R.J. Nijboer, G. van Diepen	Date of issue: 2012-06-26 Kind of issue: public	Scope: Doc.id:	
	Status: final Revision nr: 1.0		

Authors: R.J. Nijboer, G. van Diepen	Date of issue: 2012-06-26 Kind of issue: public	Scope: Doc.id:	
	Status: final Revision nr: 1.0		

1 Introduction

The goal of the software JRA ALBiUS is to provide the software tools needed to fully exploit the emergence of new and upgraded telescopes, such as e-MERLIN, ALMA, LOFAR, and APERTIF. These new telescopes will result in an explosion of data rates, and an expansion in the continuum spectral window of one to two orders of magnitude. The enormous output data rates of this new generation of instruments will provide an entirely new set of challenges for data processing, with automated processing and access to distributed computing environments becoming essential. While dealing with these challenges the aim is to make good use of the existing software packages like CASA, which is used by both ALMA and LOFAR and by individual astronomers. Both ALMA and LOFAR are focused on data-stream processing in systems based on the CasaCore library.

A limitation of existing software implementations for Calibration and Imaging is that the underlying model assumes that a single calibration factor is applicable across the instantaneous field of view of the interferometer. This assumption does not hold for the large fields of view and/or large fractions of the primary beam which will be observed by LOFAR, ALMA and APERTIF and which are becoming available for the EVN, e-MERLIN and EVLA as the correlator capabilities of those instruments are enhanced. Polarization imaging over wide fields of view presents additional challenges for all these instruments. In particular, the polarization response of the dipole arrays used by LOFAR will have strong direction dependence.


Image plane effects can be corrected using some of the more modern imaging algorithms, which are currently being developed, but the algorithms will require enhancements to fully incorporate the required direction dependence. The goal within subtask 6.2.5 is to extend the software implementation for primary beam correction to the most general case where polarization effects are incorporated and the various dishes or stations may have different primary beams. Moreover, the software implementation will be made demonstrated in a modern, distributed computing environment. For this the LOFAR computing environment is used as the development platform.

In chapter 2 an overview of various direction dependent effects and ways to correct for them is presented. Rather than giving an in depth analysis of these effects and correction methods we introduce them and provide references to the appropriate literature for further reading. From chapter 2 we conclude that projection methods are currently the most efficient way to correct for direction dependent effects. We, therefore, focus on a projection method to correct for non-coplanar baseline effects and primary beam effects: AW-Projection. Chapter 3 describes the extended AW-Projection algorithm, while chapter 4 provides a manual for the implementation of the algorithm in the CASA framework. In chapter 5 future improvements in the implementation are discussed as well as extensions to correction for direction dependent ionospheric effects. We conclude this report with conclusions in chapter 6.

1.1 Acknowledgements

This work was performed in close collaboration with Cyril Tasse (Observatoire de Paris), Bas van der Tol (Leiden University), Joris van Zwieten (Science & Technology), and Sanjay Bhatnager (NRAO). We thank Francesco de Gasperin (Max-Planck-Institut fuer Astrophysik) and Alexander Shulevski (Kapteyn Astronomical Institute) for their help with testing the AWImager implementation.

This report is a deliverable for subtask 6.2.5 of the ALBiUS project, a Joint Research Activity under the RadioNet FP7 program. The work is supported by the European Community Framework Programme 7, Advanced Radio Astronomy in Europe, grant agreement no.: 227290.

Authors: R.J. Nijboer, G. van Diepen	Date of issue: 2012-06-26 Kind of issue: public	Scope: Doc.id:	
	Status: final Revision nr: 1.0		

2 Direction Dependent Effects

When observing with an array of radio receivers (antenna's, dishes, aperture arrays ...) the measured signal gets perturbed by a number of effects. When calibrating the array for these effects it is generally assumed that these effects are receiver based (although there are ways to deal with non-receiver based effects like closure errors). Each receiver based effect in turn can be considered to be a multiplication of direction independent effects and direction dependent effects. Traditionally in radio astronomy only direction independent effects were needed to be calibrated and corrected for, like amplitude gain, phase, or "leakage" effects. With new instruments like LOFAR, ALMA, and the upcoming ASKAP, MeerKAT, and SKA telescopes as well as the upgrade of existing instruments like the EVLA, and e-Merlin that aim at reaching higher sensitivities and / or image wide field of views the calibration and correction of direction dependent effects becomes ever more important. In this section we summarize the three most important direction dependent effects: non-coplanar baselines, primary beams, and ionosphere. A more in depth description of calibration and imaging (i.e. correction) of radio interferometric data can be found in [1], [2], [3], and [4].

The correction for non-coplanar baselines is well known and is implemented in e.g. CASA by means of the w-projection method [5]. We discuss the W-Projection algorithm in the next section, since the convolutional correction approach for the primary beam derives from this W-Projection method [6]. The direction dependent effect caused by the primary beam is probably the dominant direction dependent effect in most applications. In the ALBiUS project we have focussed on correcting for the primary beam effect. The ionosphere is also discussed here, but the implementation of a correction method for ionospheric effects is outside the scope of the ALBiUS project. This is future work and it is further discussed in chapter 5.

The response of a radio telescope can be described by the Measurement Equation [7], [1]:

$$\mathbf{V}_{ij}^{Obs}(f, t) = \mathbf{M}_{ij}(f, t)W_{ij} \int \mathbf{M}_{ij}^s(\mathbf{s}, f, t)\mathbf{I}(\mathbf{s}, f, t)e^{-2\pi i(\mathbf{b}_{ij}\cdot\mathbf{s})}d\mathbf{s},$$

where \mathbf{V} denotes the measured visibility, \mathbf{b} denotes the baseline vector (i.e. the vector between receptor i and receptor j), \mathbf{I} denotes the sky vector, W denotes a weighting factor, and \mathbf{M} and \mathbf{M}^s denote the direction *independent* and direction *dependent* gains respectively. This is the Measurement Equation in its most general form. When calibrating and correcting for certain effects it reduces to a more specific form.

2.1 Non-coplanar baselines

Neglecting any instrumental effects for now, the measurement equation reduces to [5]


$$\mathbf{V}_{ij}^{Obs}(u, v, w) = \int \frac{\mathbf{I}(l, m)}{\sqrt{1-l^2-m^2}} e^{-2\pi i(ul+vm+w(\sqrt{1-l^2-m^2}-1))} dl dm,$$

where, u, v, w denote the baseline vector components and l and m are the corresponding sky coordinates. For short non-coplanar baselines ($w \approx 0$) or small fields of view ($l^2+m^2 \approx 0$) this equation reduces to a two dimensional Fourier transform. However, for long baselines or large fields of view the "w-term" introduces a direction dependent effect. As a result the point spread function with which the image is convolved becomes position dependent and standard deconvolution algorithms are not sufficient any more.

2.2 Primary Beams

In order to create images with true fluxes the data needs to be corrected for the attenuation by the primary beam of the receptor. In most cases primary beam correction is a prominent direction dependent effect. Although in some special cases the correction can be done after the fact, in general the correction must take place while creating the image.

The primary beam attenuation pattern varies over the field of view, making it a direction dependent effect, and it is dependent on both time and frequency. Except for telescopes with equatorial mounts (like the WSRT) or a 3D-axis (like ASKAP) the primary beam pattern will rotate over the sky during a synthesis

Authors: R.J. Nijboer, G. van Diepen	Date of issue: 2012-06-26 Kind of issue: public	Scope: Doc.id:	
	Status: final Revision nr: 1.0		

observation. Since the primary beam pattern is not rotationally symmetric due to e.g. projection effects in case of aperture arrays (LOFAR) or non-colocated feeds (EVLA) this rotation will generate a time dependent effect. For wide frequency bands the primary beam pattern will also vary with frequency.

Apart from the time and frequency dependence the primary beam needs to be treated in full polarization, i.e. as the combination of two voltage beams. This is the case for an aperture array like LOFAR where this is a major effect, but also for instruments like the EVLA in case high dynamic range images are to be created. And in case of heterogeneous arrays, like eMerlin, ALMA, and LOFAR, the data processing needs to correct for different primary beam patterns for the different type of receivers.

On top of all these effects there may be instrumental errors, like pointing errors, adding to the time, frequency, and spatial variations. These errors need to be determined in a calibration step prior to the imaging step or, more accurately, these errors need to be determined iteratively between calibration and imaging steps. Calibration for pointing error has been reported on in [6] and [8]. For the work reported here we assume the primary beam pattern as known (either from a model or as a result of a calibration step) and we use the pattern to construct a primary beam corrected image.

2.3 Ionosphere

Fluctuations in the Total Electron Content (TEC) of the ionosphere introduce time variable direction dependent effects. There are two main effects [9]:

- A direction dependent phase component which results in a “moving” source in the sky. If not properly corrected for the source gets “blurred” in the image: it becomes extended and the peak flux drops. In extreme cases it will completely decorrelate.
- A direction dependent rotation of the polarization vector called Faraday rotation.

The effect of the ionosphere will be stronger at lower frequencies and its direction dependent effect will show up more in wide fields of view. In principle there will be four different situations depending on the field of view, the baseline length, and the ionospheric scale length, see Figure 1. Direction dependent ionospheric calibration and correction is needed in situations 3 and 4.

With LOFAR so far three main components of ionospheric fluctuations have been found [10]:

- the diurnal cycle, which yields a long term temporal phase variation,
- Traveling Ionospheric Disturbances (TIDs), which have a periodic spatial and temporal behaviour, and
- Kolmogorov turbulence, which yields small scale fluctuations.

Correcting for ionospheric effects is outside the scope of this report. It is, however, part of the future work that is needed to properly deal with all direction dependent effects. It is therefore important that any correction method for the primary beam can be extended to ionospheric effects.

Authors: R.J. Nijboer, G. van Diepen	Date of issue: 2012-06-26 Kind of issue: public	Scope: Doc.id:	ASTRON
	Status: final Revision nr: 1.0		

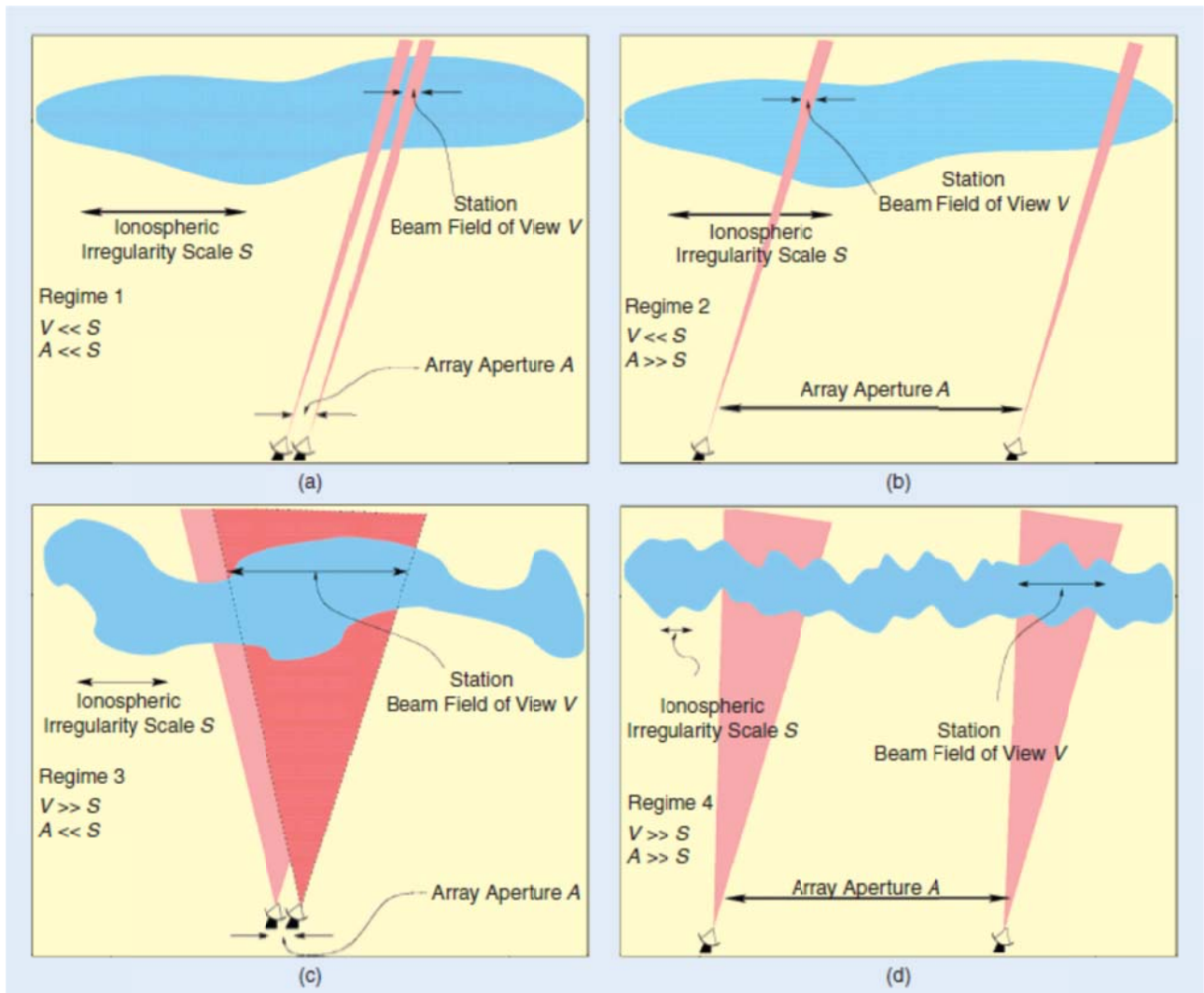



Figure 1 Four situations depending on Field of View, V , baseline length, A , and ionospheric scale length, S , [11]. Figure courtesy of Wijnholds et al. [4].

2.4 Correction methods

When making an image it should be corrected for direction dependent instrumental effects, like primary beam and ionosphere, as described in the previous sections. There are various methods to construct an image: Least Square Imaging approaches [12], Direct Fourier Transform [13], Facets (both image based and uv-based) [13], and projection methods [5]. All these methods can be used (or can be extended to be used) for making images that are corrected for direction dependent effects.

In Least Squares Image Estimation the image pixels are fitted to the uv-data in a weighted sense. In this way both image plane and visibility plane effects can be treated in an accurate way. The total amount of processing needed, however, scales with the total number of pixels to the third power [14]. Therefore, the application is computationally expensive and it is only feasible to use it for low resolution images.


The Direct Fourier Transform (DFT) is described by a transformation from each visibility sample to each pixel. The method is computationally far more expensive than Fast Fourier Transform (FFT) based methods. Therefore, FFT based methods are used in traditional radio astronomical imaging applications.

Authors: R.J. Nijboer, G. van Diepen	Date of issue: 2012-06-26 Kind of issue: public	Scope: Doc.id:	
	Status: final Revision nr: 1.0		

Both facet based methods and projection based methods are using FFTs in the image construction. When correcting for direction dependent effects in the facet approach the image is divided up into a number of facets (i.e. smaller images) and the data is corrected for each facet. This correction is exact for the center of the facet and degrades towards the edge of the facet. By making the facet size small the error can be minimized at the expense of additional computation. This approach is implemented in AIPS [15] and CASA [16]. The AIPS implementation was extended to not only correct for w-term but also for ionospheric effects [17].

In projection methods each visibility is projected onto a 2D uv-plane, using a convolutional footprint. In this way one can correct for the w-term due to non-coplanar baselines (W-Projection, [5]), the primary beam (A-Projection, [6]), the combination of both (AW-Projection) and the method may even be extended to correct for ionospheric phase [18]. Projection methods are computationally more efficient than facet based approaches. In fact, it was shown that w-projection is the fastest way to make a w-term corrected image, assuming all computations can be done in memory and without considering any parallelization effort, [19], [5].

In the remainder of this report we describe the extension of the AW-Projection implementation in CASA to the most general case, where the correction is treated in full polarization and a heterogeneous array with different primary beams can be handled. This would make the implementation of AW-Projection available to all radio telescopes, most notably ALMA, LOFAR, eMerlin, and ultimately the SKA, provided accurate primary beam models for these telescopes are available.

Authors: R.J. Nijboer, G. van Diepen	Date of issue: 2012-06-26 Kind of issue: public	Scope: Doc.id:	
	Status: final Revision nr: 1.0		

3 Implementation of AW-Projection

The CASA package contains software (as a C++ framework) to create images from visibility data. Not only does it create an image by Fourier transforming the visibility data, but it also deconvolves the image [13]. Deconvolution is implemented by iteratively, in major and minor cycles, applying and inverting the Measurement Equation. In the forward step visibilities are predicted from the current sky image. This step uses the Measurement Equation and can be performed with high accuracy, i.e. as accurate as the underlying models for direction dependent effects will allow. The backward step inverts the Measurement Equation and is generally performed by approximation. Since the deconvolution approach is iterative, any inaccuracies in the backward step may be corrected for in the forward step.

In the Imaging approach two operations are important:

1. Gridding of the visibility data to a regular grid that is then Fourier transformed to an image (backward step);
2. Degriding of the (model) visibility data obtained from the Fourier transform of an image (forward step).

The gridding and degidding steps are encapsulated in a base class from which classes can be derived which calculate direction-dependent corrections and (de)convolve the visibility data with them. CASA supports the following corrections:

- W-term to handle non-coplanar baselines.
- A-term to handle beam effects. At the moment CASA can only handle an antenna beam that is the same for all antennae, but that can vary with parallactic angle. Polarization effects are currently neglected.

The Measurement Equation for Primary Beam correction can be written as

$$\mathbf{V}_{pq} = (G_q^* \otimes G_p) \text{FT} \left[(\mathbf{E}_q^* \otimes \mathbf{E}_p) \exp \left(-2\pi i w_{pq} \left(\sqrt{1 - l^2 - m^2} - 1 \right) \right) \right] * \int \mathbf{I}(l, m) \exp \left(-2\pi i (u_{pq} l + v_{pq} m) \right) dl dm,$$

where the Kronecker product of the \mathbf{E} Jones matrices is a 4 by 4 Mueller matrix describing the Primary Beam term and * denotes the convolution operator. In the existing CASA implementation all \mathbf{E} Jones matrices should be equal and the off-diagonal matrix elements of the Mueller matrix that they generate are neglected, hence neglecting polarization (leakage) effects. The current work generalizes this approach to a treatment of the full Mueller matrix that may be constructed from non-equal Primary Beam patterns.


The existing CASA framework can be generalized by implementing a few extra classes. Extending the CASA framework has been done in collaboration with NRAO, where CASA is developed. NRAO uses the extended framework as a basis for EVLA and ALMA data processing. In addition to extending the existing framework we also focus on implementing some LOFAR specific classes.

The program AWImager has been written on top of the CASA framework to implement the AW-Projection for the LOFAR case. Currently it can only handle the multi-frequency synthesis case where all data of the given channels are imaged to a single image. The basic implementation of the software will be described in the next section. In the section thereafter important optimizations (e.g. splitting array and element beam) are discussed to make the program much more efficient. The final section of this chapter presents test results.

3.1 Extending the CASA implementation

In order to extend the existing CASA implementation to the most general case several issues have to be addressed:

1. The primary beam differs per station;
2. The primary beam varies with time and direction;

Authors: R.J. Nijboer, G. van Diepen	Date of issue: 2012-06-26 Kind of issue: public	Scope: Doc.id:	
	Status: final Revision nr: 1.0		

3. The signal leaks from one polarization to another, so the off-diagonal terms of the Jones matrices of both stations cannot be neglected. In order to handle the full Stokes correctly, a Mueller matrix with 16 elements has to be used instead of the 4 diagonal elements only;
4. For the low frequencies used by LOFAR the ionosphere results in phase changes that cannot be neglected. They vary with time and direction;
5. The ionosphere gives rise to Faraday rotation varying with time and direction. It also requires all 16 Mueller elements to handle the Stokes correctly;

The extensions to the CASA framework that are needed to address the above issues are not only relevant for LOFAR, which could be seen as the worst case telescope, but are also required by other telescopes like eMerlin, eVLA, and ALMA, for high dynamic range imaging. This is in particular true for the first three issues.

Aforementioned direction-dependent effect corrections can be combined in the A-term of the 2-dimensional convolution functions used when (de)gridding the visibility data. For the LOFAR case the convolution functions have to be calculated per baseline for a given time range (down to 5 minutes for the primary beam and possibly down to 1 minute for the ionosphere). The convolution functions can be assumed to be constant for these time ranges. Note that the W-term of a baseline varies on much longer timescales and can therefore assumed to be constant for such periods of time.

In the calculation of a convolution function the W-term has to be combined with the A-term for each station pair. It should be noted that the size of the footprint for the W-term is much larger than the size for the A-term. Because the W and A terms have to be multiplied in the image domain, they have to be convolved in the visibility domain. That can be done in two ways:

- The current implementation FFTs the terms to the image domain to be able to use simple multiplications. It requires the A-term to be zero-padded to make the sizes the same. The result is FFT-ed back to the visibility domain.
- Using a direct convolution. This is a viable option, because the size of the A-term is very small compared to the W-term size (typically 15x15 compared to 1024x1024). See section 3.3 for a more detailed discussion.

The convolution functions are calculated on the fly, because it is not feasible to cache them in memory or on disk. Thus for each major cycle in the cleaning stage the convolution functions are recalculated. However, the W-terms only depend on w-plane, so they are calculated once and cached.

3.2 Parallelised and distributed processing

Using OpenMP the compute-intensive parts of the AWImager program have been parallelised in the following ways:


1. The W-terms are calculated in parallel over w-plane;
2. For each time period the A-terms are calculated in parallel over station;
3. For each time period calculating the convolution functions and convolving the visibility data with them are done in parallel over baseline. For this purpose each thread has its own grid to sum the gridded data. At the end the grids are added together.

On a 24-core machine, this way of parallelization results in an almost linear speedup of the processing time.

In several cases the data of multiple subbands (residing on different machines) have to be combined in a single image. Currently this is done by combining those data in a single data set and processing them on a single machine. Work is underway to do the gridding step in a distributed way and to send the final grids to the master node to be added and to form the final image. The same can be done for degrading. It should also result in an almost linear speedup.

3.3 Optimization: FFT or direct convolution

Many FFTs are used in AWImager to calculate the convolution of the W- and A-term (and the necessary spheroidal tapering functions). The highly optimized FFTW package is used to do the FFTs where sizes recommended by FFTW are used to make the FFTW performance as high as possible. Furthermore,

Authors: R.J. Nijboer, G. van Diepen	Date of issue: 2012-06-26 Kind of issue: public	Scope: Doc.id:	
	Status: final Revision nr: 1.0		

precomputed FFTW wisdom for about all possible FFT sizes is used to create an FFT plan as fast as possible. This is important for two reasons:

- Creating an optimized FFTW plan can take quite some time. Precomputed wisdom turns the creation of a plan into a simple table lookup.
- Creating an FFTW plan is not thread-safe, thus cannot be used in a parallel way.

As mentioned in section 3.1 it is possible to use a direct convolution instead of FFTs. It depends on the size of the W- and A-term if this approach results in better performance. For LOFAR the A-term size is usually very small compared to the W-term size and rough back-of-the-envelope calculations show this approach is doable on a CPU. However, it has to be implemented to show if it is indeed the case. GPUs are usually very strong in convolutions, so the break-even point for them will probably be reached for larger sizes.

3.4 LOFAR Optimization: splitting array factor and element beam

In the former sections it was explained that the convolution functions needed to correct for direction dependent effects, are calculated for every few minutes of data. For LOFAR they have to be calculated for all 16 Mueller elements and for ~600 baselines. Furthermore, each visibility data point is (de)convolved with 4 Mueller elements, thus 4 (de)convolutions.

For many imaging cases, however, it is possible to reduce the amount of work drastically by taking advantage of the characteristics of the LOFAR beam. It can be split into two parts:

1. The element beam is the beam of each individual element (LBA dipole or HBA tile) in the station. The core and remote LOFAR stations are constructed such that all elements in them have the same orientation, thus the same element beam. (Note that this breaks down for the international stations due to the curvature of the Earth destroying the parallel alignment across different stations.) Furthermore, the element beam can be assumed to be constant for longer time periods (10 minutes or more) than the station beam which is dominated by the array factor. In the element beam the polarised signal leaks from each correlation into the other correlations, so all 16 elements in its Mueller matrices have to be used.
2. The array factor defines how the elements are combined to form the station beam. This is a scalar factor that varies in time. Since it is scalar, it has no polarisation leakage and, hence, all off-diagonal elements in its Mueller matrices are zero.

Very often a LOFAR image will be made from data in which the international stations are discarded. It is clear that for these cases the Mueller matrices can be split into two parts.

1. The array factor part can be calculated and applied for each baseline and for each few minutes of data. Because only the diagonal elements need to be used, it is four times cheaper than having to do it for all Mueller elements.
2. The element beam part can be calculated every 10 minutes (or more) of data. Only a single Mueller matrix (with all 16 elements) needs to be calculated, because it does not depend on baseline. This Mueller matrix has to be applied to the gridded result of the convolutions of the array factor matrices and the data for those 10 minutes.

Applying the element beam correction to the gridded data can be done in two ways.

1. In the image domain the correction matrices for the two beam parts have to be multiplied, thus in the Fourier plane they have to be convolved. It means that the element beam matrix has to be convolved with the summed result of the convolution of the array factor matrices and the data for that period 10 minutes. The final result can be added to the final data grid. The convolution can be optimized, because the summed result will contain many zeroes.
2. Another way to apply the element beam correction is doing it in the image domain. In this way the FFT-ed data grid can be multiplied with the correction and added to the final image. No FFTs are needed to calculate the Mueller elements and no convolution has to be done. However, the summed result has to be FFT-ed for every 10 minutes, which can be expensive.

Authors: R.J. Nijboer, G. van Diepen	Date of issue: 2012-06-26 Kind of issue: public	Scope: Doc.id:	ASTRON
	Status: final Revision nr: 1.0		

The current implementation in the LOFAR imager uses the first method, because it lends itself better for parallelization. It has not been tested yet how its performance compares to the second method.

3.5 LOFAR Optimization: ignoring very high w-values

The AWImager has the ability to ignore data with very high values for w . Such data are very compute-intensive because of the large sizes of the convolutional footprint that correspond to these high w -values. The highest values for w are obtained by observing towards low elevation. Baselines having large w values then result in short projected baselines. Since LOFAR already has many short baselines, ignoring these baselines does not degrade the final image much.

3.6 Test results

In order to test the performance of the AWImager implementation various tests have been performed both on simulated data and on real LOFAR data. This section describes the results from some of these tests.

3.6.1 Simulation of one off-axis source

This test was performed by Cyril Tasse [20].

A single off-axis source with values $IQUV = (100,40,20,10)$ was simulated using the Calibration software package BBS [21] to simulate the data. The simulation was based on an 8 hour data set, it included a model for the LOFAR primary beam, and the corresponding convolution functions were updated every 10 minutes.

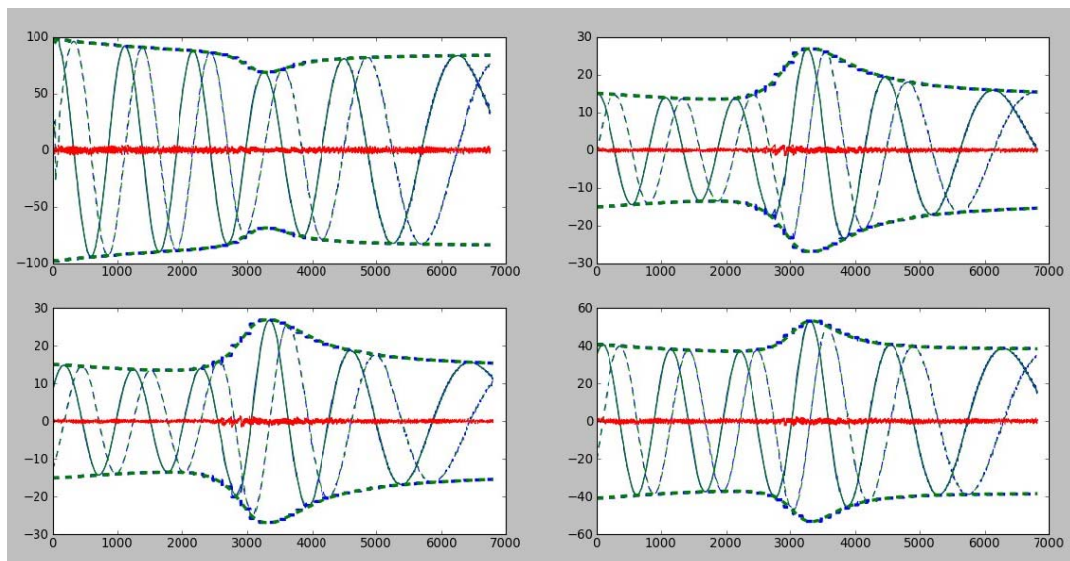


Figure 2 Comparison of AWImager de-gridding (blue) step against BBS Predict (green) step: top left XX, top right XY, bottom left YX, and bottom right YY.

Figure 2 shows the comparison between the BBS Predict (green) that uses a Direct Fourier Transform and the AWImager de-gridding (blue). The agreement between both packages is excellent. In Figure 3 a close-up of the comparison for the YY signal is shown. The small discrete steps are due to the nearest neighbour interpolation oversampling that is used inside the algorithm. The large scale discrete steps are due to the update rate of the convolution functions for the Primary Beam. The flux of the source was recovered better than 1%.

Authors: R.J. Nijboer, G. van Diepen	Date of issue: 2012-06-26 Kind of issue: public	Scope: Doc.id:	ASTRON
	Status: final Revision nr: 1.0		

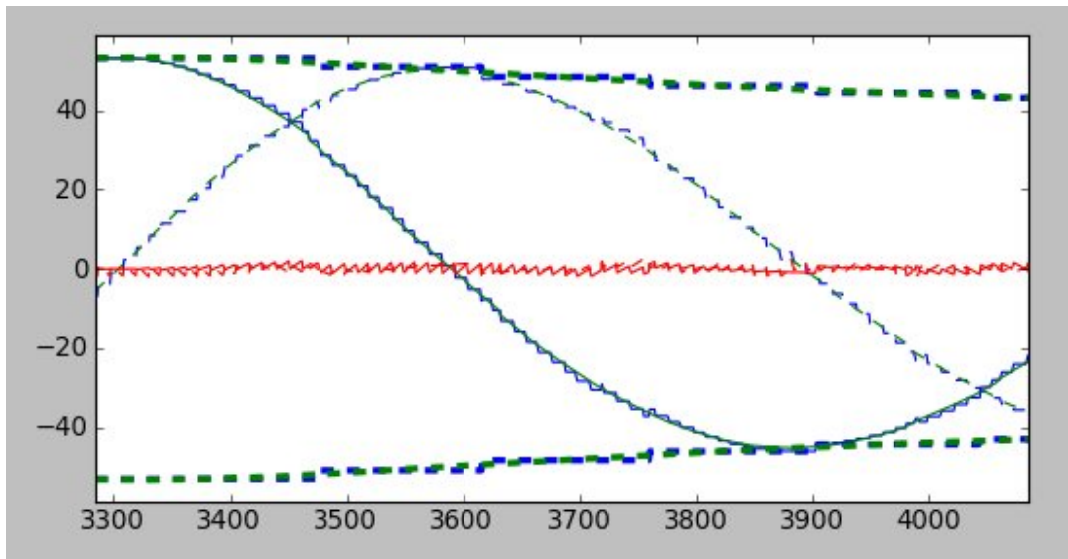


Figure 3 Close up of the YY comparison of Figure 2.

3.6.2 Simulation of 10 sources

This test was performed by Francesco de Gasperin and Cyril Tasse [22].

Using BBS 10 sources were simulated: one 10 Jy source in the center of the field and nine 1 Jy sources on a spiral out to a distance of 5 degrees, see Figure 4. All sources are unpolarized. The simulation was based on an 8 hour LBA dataset in the direction of VirA.

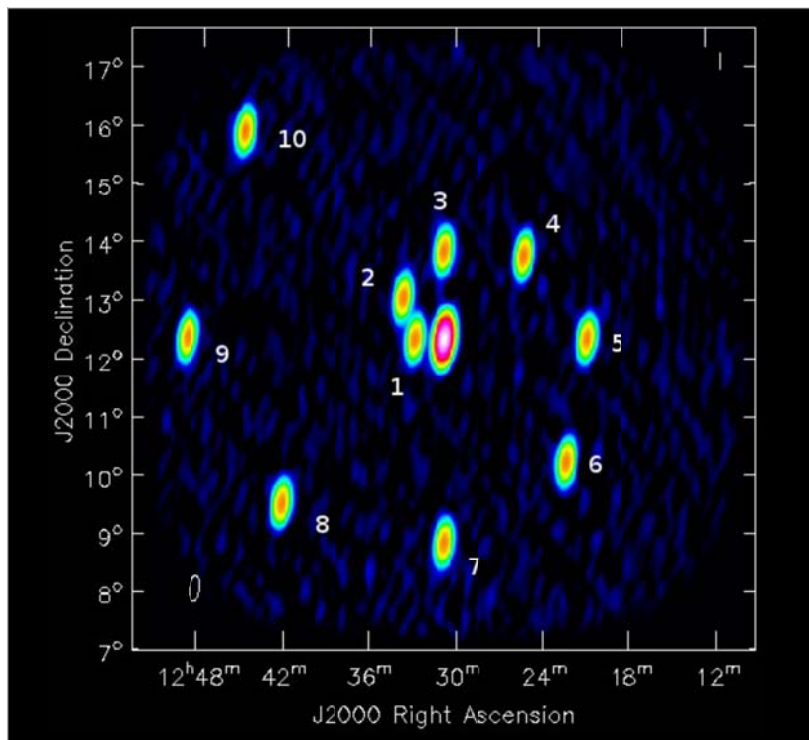



Figure 4 Image of the simulated data. The central source is 10 Jy; the other sources 1 Jy each. All sources are unpolarized.

Authors: R.J. Nijboer, G. van Diepen	Date of issue: 2012-06-26 Kind of issue: public	Scope: Doc.id:	
	Status: final Revision nr: 1.0		

In Table 1 the recovered fluxes by the AWImager with and without beam correction are shown. It is clear that the beam correction improves the recovered flux values. The total error is of the order of 1% to 3%. This error level is probably due to deconvolution effects. The recovered values for QUV were 0 within the numerical noise.

1	1.031835e+00	1.031839e+00
2	9.992662e-01	1.012118e+00
3	1.012191e+00	1.045775e+00
4	1.014027e+00	9.992201e-01
5	9.974497e-01	9.501189e-01
6	1.003099e+00	8.812889e-01
7	9.966373e-01	8.453111e-01
8	9.966382e-01	8.283383e-01
9	1.003011e+00	8.758132e-01
10	1.031732e+00	9.991207e-01

Table 1 Recovered fluxes for 10 simulated sources. Second column are beam corrected values, third column are values that are not corrected for the primary beam.

The same dataset was used to test a Self-Cal cycle. The sky model started with only the central source. After a few cycles the other sources were retrieved at the correct flux. 2 to 5 % of the total source flux, however, did leak into the QUV components.

3.6.3 Simulation of many sources

This test was performed by Cyril Tasse.

Simulated visibility data have been generated with the BBS program from a source model of a wide field containing several tens of sources. The predicted data included the effect of the LOFAR primary beam model. Subsequently a restored image of those data was made in various ways as shown in Figure 5:

- CASA imager where only the W-term could be corrected for (top left);
- AWImager; where only the array beam is corrected for (top right);
- AWImager; where the array and element beam are corrected for (bottom left).

Authors: R.J. Nijboer, G. van Diepen	Date of issue: 2012-06-26 Kind of issue: public	Scope: Doc.id:	ASTRON
	Status: final Revision nr: 1.0		

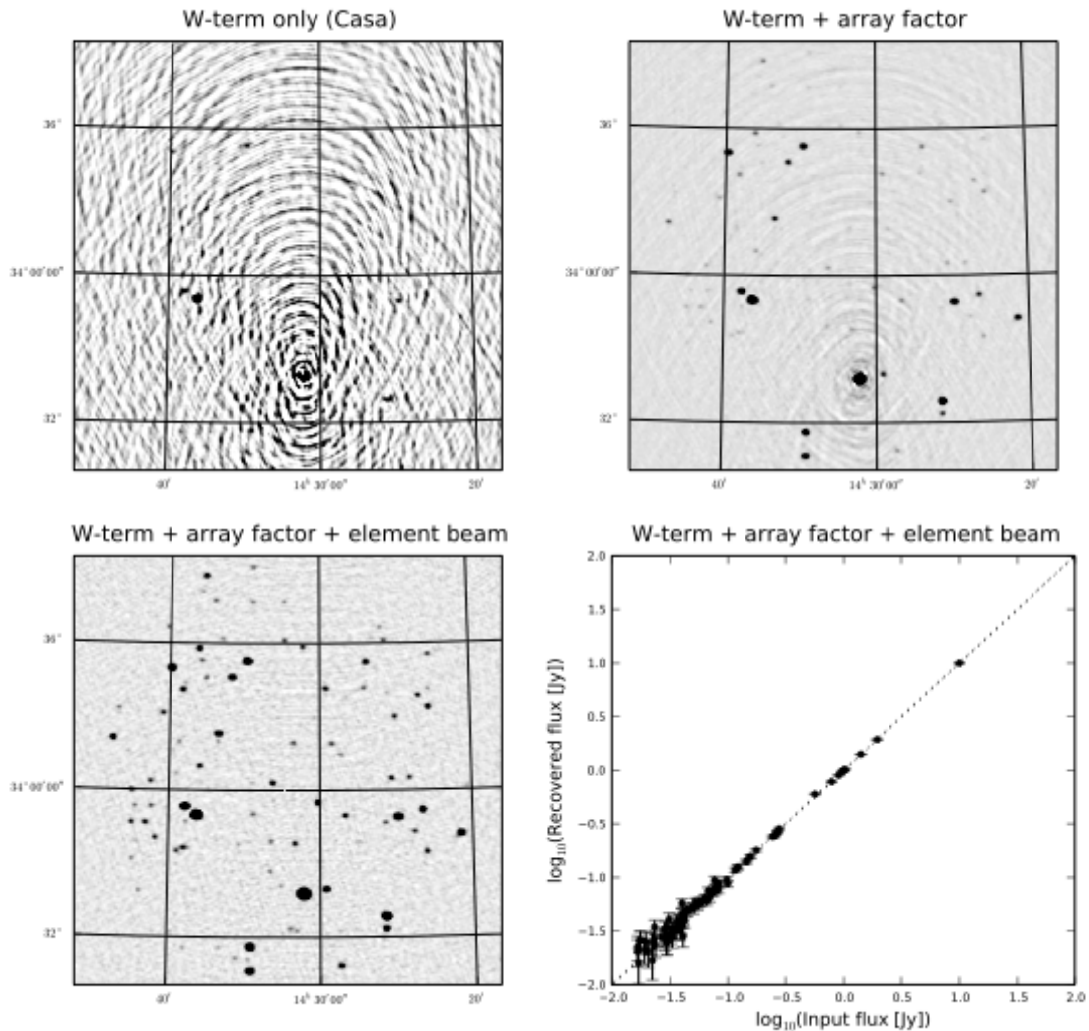



Figure 5 Wide field corrected images for w-term only (top left), w-term + array factor (top right), w-term + array factor + element beam (bottom left) and the recovered fluxes for the last image as compared to the original fluxes (bottom right).

It is clear that correcting for the array factor only already improves the image dramatically. From the images created with the AWImager it is also clear that additional correction for the element beam further improves the image. Hence, it is important to take the off-diagonal Mueller elements into account.

The bottom right picture shows the fluxes of the sources found in the beam corrected image (array factor + element beam) compared to the original fluxes used in the simulation model. It shows that the original fluxes are recovered very well, thus that the beam correction works well.

3.6.4 Tests on real data


Tests of the AWImager that were performed on real LOFAR data were all inconclusive so far. Results that were obtained by using CASA software and w-projection only were as good as results using AWImager and

Authors: R.J. Nijboer, G. van Diepen	Date of issue: 2012-06-26 Kind of issue: public	Scope: Doc.id:	
	Status: final Revision nr: 1.0		

aw-projection. This is still an area of active investigation. The lack of improvement on real data may be explained by a number of things:

1. The LOFAR primary beam that is produced in hardware does not match the beam model.
 - a. Due to synchronization problems within a LOFAR station the station beamformer does not fully focus the primary beam. This means that the beam that is created does not match the beam model that is used with BBS and the AWImager. After this problem is fixed the station calibration tables need updating in order to get a properly functioning beamformer.
 - b. It was recently found that the current beam model (bandpass) has its resonance peak at a different frequency as the one determined from the data. The current explanation for this is that the beam simulations on which the model is based do not include the effect of the Low Noise Amplifier (LNA). Currently new simulations are underway to verify this assumption and if true to determine an improved beam model.
2. The current images may still be limited by (Self-) Calibration inaccuracies. Low frequency observations using aperture arrays are a completely new observing regime. Therefore, finding the best way to calibrate the system is still an area of active research. Moreover the calibration routines also make use of a beam model, which currently has its limitations, see point 1.

Since the AWImager produces good results on simulated data, its performance on real data is likely to be explained by the above facts that are external to the AWImager implementation.

Authors: R.J. Nijboer, G. van Diepen	Date of issue: 2012-06-26 Kind of issue: public	Scope: Doc.id:	
	Status: final Revision nr: 1.0		

4 Code manual

In this section we will describe the necessary steps needed to perform successful imaging of LOFAR data using the AWImager. Note that the AWImager remains under development. Therefore this documentation is very dynamic. The most up to date version of this manual can be found as part of the LOFAR Imaging Cookbook that can be found on the ASTRON web pages [23]. The manual refers to the installation of the software on the LOFAR Central Processing clusters.

4.1 Background

The AWImager is specially adapted to image wide fields of view, and imaging data produced by non-coplanar arrays, where the W term in the measured visibilities is not negligible. Furthermore, AWImager corrects for direction dependent effects (LOFAR primary beam) varying in time and frequency. The used algorithm is AW-Projection.

The algorithm is implemented using some CASA libraries. In the future it will become available in the CASA software through NRAO.

4.2 Usage

To run AWImager, you first need to setup your environment using:

```
use LofIm
```

Before running AWImager, it is necessary to calibrate the dataset and correct the visibilities towards the phase center of the observation. This can now be done by not specifying any direction in the *correct* step of BBS.

```
Step.correct.Model.Sources = []
```

AWImager can run in a parallel fashion. The number of processing cores to be used during imaging can be specified in an environment variable:

```
export OMP_NUM_THREADS=n
```

If not specified, all cores will be used.

AWImager is quite memory hungry, so the number of cores should be limited in case it fails due a 'bad alloc' error.

4.3 Output files

AWImager creates several image output files. Note that in the following list `<image>` is the image name given using the `image` parameter.


- `<image>.model` is the uncorrected dirty image.
- `<image>.model.corr` is the dirty image corrected for the average primary beam.
- `<image>.restored` and `<image>.restored.corr` are the restored images.
- `<image>.residual` and `<image>.residual.corr` are the residual images.
- `<image>.psf` is the point spread function.
- `<image>0.avgpb` is the average primary beam.

Furthermore, a few other files might be created for internal use in AWImager.

4.4 Parameters

An extensive list of the parameters that can be used by the AWImager can be obtained by typing:

```
awimager -h
```

Authors: R.J. Nijboer, G. van Diepen	Date of issue: 2012-06-26 Kind of issue: public	Scope: Doc.id:	
	Status: final Revision nr: 1.0		

Eventually, to run the imager, you can type:

```
awimager ms=test.MS image=test.img weight=natural wprojplanes=64
npix=512 cellsize=60arcsec data=CORRECTED DATA padding=1. niter=2000
timewindow=300 stokes=IQUV threshold=0. operation=csclean
```


which is one command spread over multiple lines.

It is also possible to specify these parameters in a parset and run it like:

```
awimager parsetname
```

Many parameters can be set for the AWImager. The most important parameters are listed below.

Parameter	Default	
Ms		name of the input MeasurementSet
Data	DATA	name of the data column to use in the MeasurementSet
image		name of the image
npix		number of pixels in the RA and DEC direction
cellsize		size of each pixel. A unit can be given at the end. E.g. 30arcsec
padding	1.	The padding factor to use when imaging. It can be used to get rid of effects at the edges of the image. If, say, 1.5 is given, the number of pixels used internally is 50% more.
stokes	IQUV	The Stokes parameters for which an image is made. If A-projection is used, it must be IQUV.
weight		weighting scheme (uniform, superuniform, natural, briggs (robust), briggsabs, or radial)
robust		robust weighting parameter
wprojplanes		number of W projection planes to use
maxsupport	1024	maximum of W convolution functions
oversample	8	oversampling to use for the convolution functions
wmax		ignore baselines whose w-value exceeds wmax (in meters)
uvdist		ignore baselines whose length (in wavelengths) exceed uvdist
select		Only use data matching this TaQL selection string. For example, <code>sumsqr(UVW[:2]) < 1e8</code> selects baselines with length <10km
operation		The operation to be performed by the AWImager. csclean = make an image and clean it (using Cotton-Schwab). image = make dirty image only. predict = fill the data column in the MeasurementSet by predicting the data from the image. empty = make an empty image. This can be useful if only image coordinate info is needed.
timewindow	300	width of the time window (in sec) where the AW-term is assumed to be constant (the wider the window, the faster the imager will be)
niter	1000	number of clean iterations to be done
gain	0.1	loop gain for cleaning
threshold	0	flux level at which to stop cleaning
splitbeam	true	evaluate station beam and element beam separately?

Authors: R.J. Nijboer, G. van Diepen	Date of issue: 2012-06-26 Kind of issue: public	Scope: Doc.id:	
	Status: final Revision nr: 1.0		

5 Future work

The current AWImager implementation remains under active development. On the one hand improvements in the computational speed are sought after and on the other hand the implementation will be extended towards more functionality, e.g. the correction for ionospheric effects. Ideas on these improvements are described in this section.

5.1 Further computational optimizations

There are several options to optimize the performance of the AWImager. Below some options are described that can be explored in future work.

5.1.1 GPU implementation

A very efficient GPU implementation of the W-projection algorithm has been implemented using both CUDA and OpenCL [24]. It should be tried to implement it too for the AW-projection, where the calculation of the convolution functions can be done on the GPU as well. The limited memory size of the GPU might pose a problem, especially for very large images. In such cases facets can be used to limit the image size to work on.

5.1.2 Faceting

An image can be divided into individual subimages (facets) that are combined into the total image at the tangent point of the image centre. All data have to be used for each facet, but the size of the convolution functions to use for a facet is much smaller than for the total image. The total amount of computations is not smaller, but the memory footprint can be smaller. Parallelisation can be done over facets, so each thread needs a much smaller grid than when parallelising over baseline for the total image.

Using facets might also be beneficial for GPU implementations when very large image sizes are used.

A joint deconvolution of the facets needs to be done. This is most efficiently done in the uv-based faceting approach [13]. The CASA framework already supports facets and their joint deconvolution. It has to be investigated if and how it fits in the AWImager.

5.1.3 W-stacking


The w-plane can be divided into sub-planes resulting in a stack of w-planes. The size of the W-terms in each sub-plane is much smaller, so fewer calculations have to be done. However, each sub-plane needs its own grid arrays resulting in higher memory usage. As such that is not a problem, because AWImager already uses a grid for each thread. In this way it is straightforward to parallelise over w-planes. However, the problem is to balance the load because the distribution of the visibility data over the w-planes is far from uniform. In principle it should be possible to choose the w-planes such that the amount of work to do for each plane is about equal, but it is not trivial.

5.1.4 FFT or direct convolution

As discussed in chapter 3 it needs to be investigated if a direct convolution of the A- and W-term is faster than using forward and backward FFTs. This might depend on the platform (e.g. CPU or GPU).

5.1.5 Generalization


The current implementation of AWImager uses LOFAR primary beams. However, about all LOFAR-specific code is concentrated in the class `LofarConvolutionFunction` that calculates the convolution function for the LOFAR case. By making that class overloadable (and possibly dynamically loadable), the program can be generalized towards other instruments.

Authors: R.J. Nijboer, G. van Diepen	Date of issue: 2012-06-26 Kind of issue: public	Scope: Doc.id:	
	Status: final Revision nr: 1.0		

5.2 Correction for ionospheric effects

Since the Jones matrix describing the ionospheric phase effect is essentially a scalar phase term, the effect does not cause polarization leakage and its effect can be combined with the primary beam array factor correction. The support for a convolutional kernel is limited when only the high energy content of Kolmogorov turbulence is considered. The high energy components correspond to the low spatial frequency components that generate small convolutional footprints. So it would seem possible to use a projection method for correction of ionospheric phase terms, at least in principle. The method could become impractical if the update rate becomes too fast. Initial investigations indicate that the ionospheric phase will be constant for periods of about 30 to 60 seconds. That would imply that the update rate for the ionospheric convolution functions is a factor 5 to 10 higher than for the primary beam. This makes the convolution function calculation more expensive.

The Jones matrix describing Ionospheric Faraday Rotation is a rotation matrix and therefore causes polarization leakage. Because of this the full Mueller matrix needs to be considered. Furthermore, the effect varies with time and baseline and update rates will probably be high making the correction an expensive operation. It has to be investigated whether a projection method is applicable at all (e.g. is the convolutional support finite?) and it should be investigated how the correction can be done in an efficient way. At this moment all these issues are unclear.

Authors: R.J. Nijboer, G. van Diepen	Date of issue: 2012-06-26 Kind of issue: public	Scope: Doc.id:	
	Status: final Revision nr: 1.0		

6 Conclusions


In order to fully exploit the emergence of new and upgraded telescopes, such as e-MERLIN, ALMA, LOFAR, eVLA, and APERTIF, new software tools are needed. Since this new generation of instruments produces so much data, automatic, distributed and parallel processing will be essential. Furthermore, the assumption of a single calibration factor that is constant over the full field of view will be too limiting for these instruments. Calibration and correction for direction dependent effects is needed in order to reach the high dynamic range results that these instruments are theoretically capable of.

In subtask 6.2.5 of the JRA ALBiUS we have been developing a software implementation for correction of direction dependent effects. The most important direction dependent effects are: the w -term due to non-coplanar baselines, the primary beam, and the ionosphere. Basically two ways of correcting for these effects are available: facets and projection methods. Of these two the projection methods are generally the most efficient.

In the CASA software package a projection method for correction for the non-coplanar baseline effect is available: w -projection. An algorithm for correction for primary beam by a projection method also existed (a -projection), but a general implementation was not yet available. Here we generalized the CASA implementation to correct for primary beams in the most general way: the correction is time and frequency dependent, is done while treating full polarization, and may include receptors with different primary beams. Moreover, the implementation is extendable to include correction for ionospheric effects. The resulting implementation was called AWImager.

The work on the AWImager shows that it is very well possible to correct for direction-dependent effects in the convolutional gridding step of the imager. It is, however, a very compute-intensive task and quite memory-hungry. By looking carefully at the characteristics of the instrument, it is possible to optimize considerably. However, more work is needed for further optimization, possibly dependent on the platform the program runs on.

Tests on simulated data show that the new AWImager performs well. Source fluxes are typically recovered within a few percent. Tests on real LOFAR data did not show an improved result yet as compared to not taking primary beam correction into account. The reason for this may be found in that fact that the LOFAR primary beam is not entirely understood yet and requires further characterisation and / or that the data is still limited by (self-) calibration errors.

Authors: R.J. Nijboer, G. van Diepen	Date of issue: 2012-06-26 Kind of issue: public	Scope: Doc.id:	
	Status: final Revision nr: 1.0		

7 References

- [1] Smirnov, O.M., Revisiting the radio interferometer measurement equation, I. the full-sky Jones formalism, *A&A* 527, A106, 2011.
- [2] Smirnov, O.M., Revisiting the radio interferometer measurement equation, II. Calibration and direction dependent effects, *A&A* 527, A107, 2011.
- [3] Rau et al., *Advances in Calibration and Imaging Techniques in Radio Interferometry*, IEEE Special Issue on Advances in Radio Telescopes, 2009.
- [4] Wijnholds, S.J., Van der Tol, B., Nijboer, R., Van der Veen, A.J., Calibration challenges for future radio telescopes, *IEEE Signal Processing Magazine*, p. 30, Jan. 2010.
- [5] Cornwell, T.J., Golap, K., Bhatnagar, S., The Noncoplanar Baselines Effect in Radio Interferometry: The W-Projection Algorithm, *IEEE Journal of Selected Topics in Signal Processing*, Vol. 2, Issue 5, p.647-657, Nov. 2008.
- [6] Bhatnagar, S., Cornwell, T.J., Golap, K., Uson, J.M., Correcting direction-dependent gains in the deconvolution of radio interferometric images, *A&A*, vol 486, pp. 419-429, Aug 2008.
- [7] Hamaker, J.P., Bregman, J.D., Sault, R.J., *Understanding radio polarimetry, I. Mathematical foundations*, *Astron. Astrophys. Suppl. Ser.* 117, 137-147, 1996.
- [8] Smirnov, O.M., Revisiting the radio interferometer measurement equation, III. Addressing direction-dependent effects in 21 cm WSRT observations of 3C147, *A&A* 527, A108, 2011.
- [9] Thompson, A., Moran, J., and Swenson, G. Jr., *Interferometry and Synthesis in Radio Astronomy*, Second Edition, Chapter on Ionosphere, New-York: Wiley-Interscience, 2001.
- [10] Tol, S. van der, Rottgering, H., *Ionospheric measurements with the Low Frequency Array (LOFAR)*, 13th International Ionospheric Effects Symposium, 2011.
- [11] C. Lonsdale, *Calibration approaches*, MIT Haystack Observatory, Westford, MA, Tech. Rep. LFD memo 015, Dec. 8, 2004.
- [12] Levanda, R., and Leshem, A., *Synthetic Aperture Radio Telescopes*, *IEEE Signal Processing Magazine*, vol. 27, no. 1, pp. 14–29, Jan. 2010.
- [13] Taylor, G.B., Carilli, C.L., Perley, R.A., *Synthesis Imaging in Radio Astronomy II*, ASP Conference Series, Vol. 180, 1999.
- [14] Wijnholds, S.J., *Imaging with the SKA Core*, presented at SKA 2010, 2010.
<http://www2.skatelescope.org/indico/getFile.py/access?contribId=53&sessionId=4&resId=0&materialId=0&confId=2>
- [15] Astronomical Image Processing System (AIPS). <http://www.aips.nrao.edu/index.shtml>
- [16] Common Astronomy Software Applications (CASA). <http://casa.nrao.edu/>
- [17] Intema, H., et al., *Ionospheric calibration of low frequency radio interferometric observations using the peeling scheme. I. Method description and first results*, *A&A* Volume 501, Issue 3, 2009, pp.1185-1205.
- [18] Tol, S. van der, *private communication*.
- [19] Yashar, M., Kemball, A., *Computational cost of radio imaging algorithms dealing with the non-coplanar baselines effect: I*, TDP Calibration & Processing Group memo 17, 2009.
<http://rai.ncsa.uiuc.edu/memo17.pdf>
- [20] C. Tasse, LOFAR Imager: taking Direction Dependent Effects into account using A-Projection, presented at 3CGII workshop, Albufeira, Portugal, Sept 19 – 30 2011,
http://www.astron.nl/megwiki/3GCII-Workshop?action=AttachFile&do=get&target=Tasse_3GCII.pdf
- [21] V.N. Pandey, J.E. van Zwieten, A.G. de Bruyn, R. Nijboer, *Calibrating LOFAR using the Black Board Selfcal system*, *Low Frequency Radio Universe*, ASP Conference Series, Vol. 407, 2009, Eds: D. J. Saikia, D. A. Green, Y. Gupta and T. Venturi.
- [22] http://www.lofar.org/wiki/lib/exe/fetch.php?media=public:degasperin_bwed26oct2011.pdf
- [23] R. Pizzo (editor), *The LOFAR Imaging Cookbook: Manual data reduction with the Imaging Pipeline*, <http://www.lofar.org/operations/doku.php?id=commissioning:cookbooks>
- [24] J.W. Romein, *An Efficient Work-Distribution Strategy for Gridding Radio-Telescope Data on GPUs*, ACM International Conference on Supercomputer (ICS'12), Venice, Italy, June, 2012.
<https://www.astron.nl/~romein/papers/ICS-12/gridding.pdf>